

# Feedforward compensation of scan-induced disturbances for a high-precision robotic 3D measurement system

Daniel Wertjanz, Thomas Kern, Ernst Csencsics and Georg Schitter

**Abstract**—This paper proposes a feedforward compensation approach of scan-induced disturbances to improve the uncertainty of an active-sample tracking 3D measurement module. The measurement module acts as a robotic end-effector and is designed for precise robotic measurement applications directly in the vibration-prone environment of an industrial production line. By means of a feedback control-induced stiff link, a constant position of the electromagnetically levitated measurement platform (MP) is maintained with respect to the sample surface under test. Precise 3D imaging is enabled by scanning the measuring light spot of a 1D confocal chromatic sensor with a 2D fast steering mirror (FSM). Disturbances are caused due to scanning-induced reaction forces on the MP, impairing the system's sample-tracking and 3D measurement performance. Based on the identified disturbance dynamics, a tailored feedforward control is designed to compensate the causing reaction forces. To experimentally evaluate the system performance, 3D measurements at the maximum frame of 1 fps are performed with disabled and enabled feedforward control. Evaluating the experimental results, the sample-tracking error in the MP's translational degree of freedom  $z$  is significantly reduced by a factor of 7 down to 42 nm rms, being close to the MP's static positioning noise. The reduced sample-tracking error further enables a higher 3D measurement performance, reducing the structural height uncertainty by 36% down to 180 nm rms.

## I. INTRODUCTION

Besides novel production plants and automated assembly techniques, inline quality inspection is considered as the most important prerequisite for future production [1], [2]. Flexible, fast and precise inline measurement systems are highly demanded [3], [4], as they can provide a continuous and 100% quality monitoring of industrially produced goods, enabling realtime optimization of production parameter settings to significantly increase product reliability and quality as well as the overall throughput and the production yield [5], [6]. In particular, precise inline 3D measurements on freeform surfaces [7] are a key technology for future production of structures in the single- to sub-micrometer range, with application fields ranging from the semiconductor to the automotive and consumer electronics sector [4], [8], [9].

A fast and flexible alignment of a 3D measurement tool (MT) at arbitrary measurement locations on a sample surface can be achieved by employing industrial robots [10]. However, robots themselves are not suitable for the demanded 3D surface measurements with single- or sub-micrometer resolution [11], as they are lacking the required high positioning precision. Currently, industrial robots achieve a precision

of several tens of micrometers [12], limiting the achievable resolution of conventional robotic 3D measurement systems. Modern robot-based 3D measurement systems achieve resolutions down to 50  $\mu\text{m}$  [13], [14].

Similar to the limited positioning precision of an industrial robot, another challenge of integrating a precision 3D MT directly into an industrial production line are environmental vibrations, which may cause relative motion between the MT and the sample surface. Due to motion blur, 3D measurements are corrupted on the micrometer scale [15], which is why precision quality monitoring is typically conducted in vibration-free lab environments. Consequently, a 100% quality control of goods with structural sizes in the single-micrometer range is usually not feasible without impairing the production throughput.

Aiming to tackle these challenging limitations, an active sample-tracking measurement system for precise robotic inline 3D surface inspection has been reported recently [16], [17]. In this concept, the electromagnetically levitated and actuated measurement platform (MP) maintains a constant alignment of the embedded compact and lightweight scanning confocal chromatic sensor (SCCS) [18] in six degrees of freedom (DoFs) relative to the sample surface to be inspected. With integrated tracking sensors (TSs) measuring the SCCS's position relative to the sample surface, a feedback (FB) control-induced and contactless stiff link between SCCS and sample is established. Thus, disturbing relative motion is compensated and local lab-like conditions are established, enabling 3D measurements on the sub-micrometer scale directly in a vibration-prone environment.

However, considering the SCCS' design [18], the center of mass of the integrated 2D fast steering mirror (FSM) and its pivot point do not coincide. Consequently, disturbing forces and torques on the levitated MP are induced when performing a scanning motion with the FSM, which impedes the sample-tracking performance and uncertainty. As the FSM scanning trajectory is known upfront, the resulting disturbances are of deterministic nature. Hence, the application of feedforward (FF) control techniques appears as a valid approach to compensate these disturbances and further improve the overall robotic 3D measurement system's performance [19]–[21]. With an appropriate identification process of the crosstalk dynamics from the FSM to the levitated MP, a decoupling of the two individually controlled multi-DoF systems is targeted [22], [23]. In this way, the resulting disturbances can be compensated instantaneously rather than by the integrated sample-tracking controller in a feedback manner.

The authors are with the Automation and Control Institute (ACIN), Technische Universität Wien, 1040 Vienna. Corresponding author: wertjanz@acin.tuwien.ac.at

The contribution of this paper is the design and implementation of a FF control architecture to significantly reduce the disturbances caused by the scanning-induced reaction forces on the sample-tracking MP, improving the overall 3D measurement uncertainty.

The remainder of this paper is structured as follows. In Section II, the system concept for precise robotic 3D measurements and the prototype setup are presented. Based on the problem formulation in Section III-A, the FSM-induced reaction forces on the MP are modelled. After identification of the real disturbance dynamics, a FF control architecture is therefore synthesized in Section IV. In Section V, the sample-tracking and 3D measurement performance improvement is experimentally evaluated. Finally, Section VI concludes this paper.

## II. MODULE FOR PRECISE ROBOTIC 3D MEASUREMENTS

In Fig. 1, the system concept for precise robotic inline 3D measurements on freeform surfaces within a vibration-prone environment is schematically illustrated for a single DoF. The measurement module is mounted as end-effector to the robot arm and comprises an electromagnetically levitated and actuated MP, in which a SCCS is embedded, capable of acquiring high resolution 3D measurements. With the robot being used for flexible and coarse alignment of the 3D measurement module, integrated TSs measure the SCCS' relative position to the sample surface  $z$ . By means of FB control, the position  $z$  is maintained constant, introducing a contactless stiff link between SCCS and sample by compensating vibration- as well as robot-induced disturbances  $z_S$ . In this way, lab-like conditions for the precision 3D MT are established directly in the challenging environment of an industrial production line.

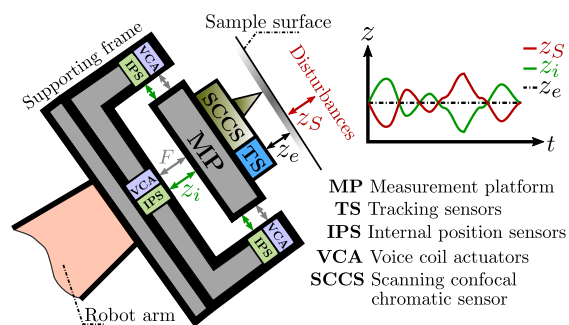
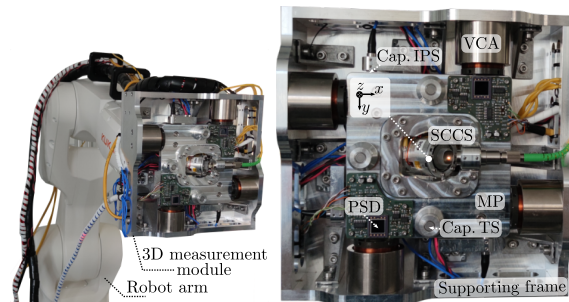


Fig. 1: System concept for precise robotic inline 3D measurements on freeform surfaces. By maintaining a constant position  $z$  between the SCCS and sample surface, disturbance-induced relative motion is actively compensated. On the top-right, the internal position signal  $z_i$  represents the motion of the actuated MP, compensating the sample motion  $z_S$ .

The system prototype with the 3D measurement module mounted to an industrial robot arm (KR 10 R900-2, KUKA AG, Augsburg, Germany) is shown in Fig. 2. In the following, the integrated active sample-tracking MP and the SCCS are discussed.



(a) Robotic 3D measurement system. (b) 3D measurement module.

Fig. 2: Robotic 3D measurement system prototype. In a), the measurement module is acting as end-effector of the industrial robot arm. b) shows the SCCS embedded into the MP, which is levitated and actuated by VCAs. IPSs measure the MP position relative to the supporting frame. The TS system used to measure the relative motion between the SCCS and a sample surface includes three capacitive sensors and two PSDs.

### A. Measurement platform for active sample-tracking

Using eight identical voice coil actuators (VCAs) for the MP's quasi-zero-stiffness actuation, a balanced system design, good decoupling between the axes as well as the system's operability in arbitrary robot poses are enabled [24]. To measure the MP's position relative to the robot arm, the measurement module comprises six capacitive internal position sensors (IPSs), enabling a FB-controlled stabilization of the MP in a free-floating position when repositioning the robot.

Three capacitive TSs are integrated in the MP to actively track a sample surface in the out-of-plane DoFs [16]. As compact, fast and precise in-plane sensors are hardly available, a position-sensitive device (PSD)-based sensor system is used to measure the MP's in-plane position relative to the sample surface. Modulated laser diodes as markers for the two PSDs are mounted together with aluminum targets for the capacitive TSs and the sample itself to a custom-made sample holder [17]. Using a single-input single-output (SISO) FB control architecture, a sample-tracking control bandwidth of 450 Hz is achieved in each DoF.

### B. Scanning confocal chromatic sensor

As can be seen in Fig. 2b, the compact and lightweight SCCS [18] is embedded in the MP. By manipulating the optical path of the high precision 1D confocal chromatic sensor (CCS) with the 2D FSM, the SCCS' measuring light spot is precisely scanned across the sample surface. The FSM is actuated by a hybrid-reluctance actuator (HRA) [25] and an  $H_\infty$  multi-input-multi-output (MIMO) FB control is applied to accurately steer the two axes of the FSM. A calibration data-based procedure is used to correctly reconstruct the 3D measurement by the two measured FSM axis deflections

and the distance measured by the CCS. In this way, the 3D measurement tool achieves a lateral and axial resolution of down to 2.5  $\mu\text{m}$  and 76 nm, respectively. Lissajous scan trajectories can be applied to the FSM axes, resulting in 3D image frame rates of up to 1 fps.

### III. PROBLEM ANALYSIS AND MODELLING

Considering the system prototype in Fig. 2b, the according CAD model of the measurement module is illustrated in Fig. 3 [16]. With the FSM's center of mass not coinciding with its pivot point, unintended reaction forces are acting on the magnetically levitated MP, which impedes the sample-tracking performance and thus, may decrease the overall 3D measurement performance.

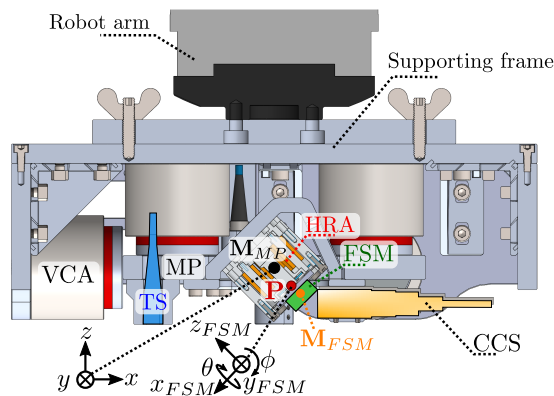


Fig. 3: CAD model of the robotic 3D measurement module. The FSM is actuated by a HRA and precisely manipulates the optical path of the CCS. The FSM's center of mass  $\mathbf{M}_{FSM}$  does not coincide with its pivot point  $\mathbf{P}$ .

#### A. Crosstalk analysis

To evaluate the effect of reaction forces caused by the FSM motion on the sample-tracking performance, the MP's sample-tracking error during the operation of the SCCS is analyzed. Considering the case for which the highest crosstalk is expected, i.e. operation at the maximum frame rate of 1 fps, Lissajous scanning frequencies of  $f_{\phi} = 59 \text{ Hz}$ ,  $f_{\theta} = 47 \text{ Hz}$  are applied to the FSM. The resulting MP's sample-tracking error is compared with the MP's static positioning error in Tab. I. As can be seen, the FSM-induced additional sample-tracking error is highest in the MP's translational DoF  $z$ , decreasing the sample-tracking performance by a factor of 10. In the remaining DoFs, the tracking error is kept close to the MP's noise floor.

To compensate the FSM-induced reaction forces in the translational DoF  $z$  of the MP, a FF control approach is considered as suitable solution. In this relation, the sample-tracking error during full-frame 3D imaging at the maximum rate of 1 fps (worst case) is targeted to be reduced to the same order of magnitude as the MP's static positioning noise obtained with disabled SCCS.

TABLE I: RMS sample-tracking error for scanning and static FSM operation.

DoF	SCCS disabled	SCCS @ 1 fps
$x$	180 nm	192 nm
$y$	240 nm	259 nm
$z$	<b>30 nm</b>	<b>290 nm</b>
$\phi_x$	0.61 $\mu\text{rad}$	0.63 $\mu\text{rad}$
$\phi_y$	1.06 $\mu\text{rad}$	1.11 $\mu\text{rad}$
$\phi_z$	8.35 $\mu\text{rad}$	8.41 $\mu\text{rad}$

#### B. Modelling of reaction forces

With consideration of the sample-tracking robotic 3D measurement system's CAD model in Fig. 3, the reaction forces caused by the operating SCCS and acting on the MP are modelled by deriving the motion of the FSM's center of mass. Therefore, two coordinate systems are introduced, one located in the MP's center of mass  $\mathbf{M}_{MP}$  ( $CS_{MP}$ )  $[x, y, z]^T$  and the other one in the FSM's pivot point  $\mathbf{P}$  ( $CS_{FSM}$ )  $[x_{FSM}, y_{FSM}, z_{FSM}]^T$ .

The FSM's center of mass  $\mathbf{M}_{FSM}$  is located at  $\mathbf{d} = [0, 0, -d_z]^T = [0, 0, -1.9 \text{ mm}]^T$  in  $CS_{FSM}$  with respect to the pivot point  $\mathbf{P}$ . As the FSM's center of mass is rotated around the  $\theta$ - and  $\phi$ -axis, fundamental rotation matrices

$$\mathbf{R}_x(\theta) = \begin{bmatrix} 1 & 0 & 0 \\ 0 & \cos(\theta) & -\sin(\theta) \\ 0 & \sin(\theta) & \cos(\theta) \end{bmatrix} \quad (1a)$$

$$\mathbf{R}_y(\phi) = \begin{bmatrix} \cos(\phi) & 0 & \sin(\phi) \\ 0 & 1 & 0 \\ -\sin(\phi) & 0 & \cos(\phi) \end{bmatrix} \quad (1b)$$

are applied to the FSM's center of mass

$$\mathbf{M}_{FSM} = \mathbf{R}_y(\pi/4) \mathbf{R}_x(\theta) \mathbf{R}_y(\phi) \mathbf{d} \quad (2)$$

in order to obtain its motion with respect to the MP's coordinate system  $CS_{MP}$ . Using Newton's third law, the reaction forces and torques acting on the MP are equal and opposite in direction with respect to the forces and torques generating the FSM's center of mass motion. Thus, the reaction forces on the MP result to

$$\mathbf{F}_{FSM,MP} = -m_{FSM} \ddot{\mathbf{M}}_{FSM}, \quad (3)$$

with  $m_{FSM} = 6.2 \text{ g}$  being the FSM's moving mass. Similarly, the torques generating the FSM's rotational motion  $\psi = [\theta, \phi]^T$  act equally and in opposite direction on the MP. Rotating the FSM's torques into  $CS_{MP}$  yields

$$\boldsymbol{\tau}_{FSM,MP} = -\mathbf{R}_y(\pi/4) \mathbf{R}_x(\theta) \mathbf{R}_y(\phi) \mathbf{E}_{3 \times 3} \mathbf{I} \begin{bmatrix} \ddot{\psi} \\ 0 \end{bmatrix} \quad (4)$$

with  $\mathbf{I} = [I_{xx}, I_{yy}, 0]^T = [254.9 \text{ g mm}^2, 253.2 \text{ g mm}^2, 0]^T$  being the FSM's moments of inertia in the pivot point with respect to  $CS_{FSM}$ . In this relation, the calculated forces and torques from Eq. (3) and (4) act as external disturbance inputs

$$\mathbf{F}_{FSM \rightarrow MP} = \begin{bmatrix} \mathbf{F}_{FSM,MP} \\ \boldsymbol{\tau}_{FSM,MP} \end{bmatrix} \quad (5)$$

on the MP dynamics, causing an unintended MP motion.

#### IV. SYSTEM ANALYSIS AND CONTROL DESIGN

Based on the findings in Section III-B, the disturbances acting on the MP caused by FSM-induced reaction forces are identified. Figure 4 presents the simplified block diagram of the integrated measurement module control scheme. Based on the measured FSM position error  $e_\psi$ , the  $H_\infty$ -MIMO controller output  $\mathbf{u}_{\text{FSM}}$  is calculated and applied to the HRA. The HRA-generated force is applied to the dynamic FSM system  $\mathbf{G}_{\text{FSM}}$ . Similarly, the measured sample-tracking error  $e_\zeta$  is applied to the SISO proportional-integral-derivative (PID) controller  $\mathbf{C}_{\text{MP}}$ . With the controller output  $\mathbf{u}_{\text{MP}}$  applied to the VCA system ( $\mathbf{K}_{\text{VCA}}$ ), the forces  $\mathbf{F}_{\text{MP}}$  are generated and applied to the dynamic MP system  $\mathbf{G}_{\text{MP}}$ .

As discussed in Section III-B, the FSM motion-induced crosstalk  $\mathbf{F}_{\text{FSM} \rightarrow \text{MP}}$  acts as external disturbance input directly on the MP dynamics  $\mathbf{G}_{\text{MP}}$ , resulting in an additional MP motion  $\zeta$ . In order to compensate this unintended motion, a FF controller  $\mathbf{C}_{\text{FF}}$  is designed subsequently.

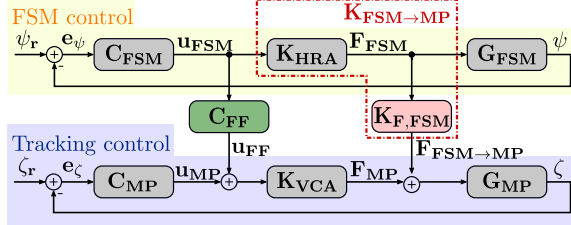


Fig. 4: Simplified block diagram of the measurement module's control scheme. The active sample-tracking control to maintain the MP's position  $\zeta$  constant is disturbed by unintended forces  $\mathbf{F}_{\text{FSM} \rightarrow \text{MP}}$  generated by the motion-controlled FSM system. A FF controller  $\mathbf{C}_{\text{FF}}$  is applied to compensate the resulting disturbances.

##### A. Identification of FSM motion-induced crosstalk

Based on the FSM's MIMO controller output  $\mathbf{u}_{\text{FSM}} = [u_\theta, u_\phi]$ , the reaction force

$$\mathbf{F}_{\text{FSM} \rightarrow \text{MP}} = \mathbf{K}_{\text{F,FSM}} \mathbf{K}_{\text{HRA}} \mathbf{u}_{\text{FSM}} \quad (6)$$

is generated and acting on the MP, which depends on the motor constant of the HRA  $\mathbf{K}_{\text{HRA}}$  as well as on  $\mathbf{K}_{\text{F,FSM}}$  including the relation from Eq. 5. As the MP is electromagnetically levitated in all DoFs, the crosstalk dynamics

$$\frac{\zeta}{\mathbf{F}_{\text{FSM} \rightarrow \text{MP}}} = \mathbf{G}_{\text{MP}} \frac{1}{\underbrace{1 + \mathbf{C}_{\text{MP}} \mathbf{K}_{\text{VCA}} \mathbf{G}_{\text{MP}}}_{\mathbf{S}_{\text{MP}}}}, \quad (7)$$

with  $\mathbf{S}_{\text{MP}}$  the sensitivity of the sample-tracking FB control, need to be measured in closed-loop operation, i.e. the MP being stabilized with respect to a sample surface. Considering constant FSM dynamics  $\mathbf{G}_{\text{FSM}}$ , the relation  $\mathbf{K}_{\text{F,FSM}} = \mathbf{K}_{\text{F,FSM}} \mathbf{K}_{\text{HRA}}$  is a static gain, yielding  $\mathbf{F}_{\text{FSM} \rightarrow \text{MP}} \propto \mathbf{u}_{\text{FSM}}$  and

$$\mathbf{K}_{\text{F,FSM}} = \frac{\zeta}{\mathbf{u}_{\text{FSM}}} \frac{1}{\mathbf{G}_{\text{MP}} \mathbf{S}_{\text{MP}}} = \text{const.} \quad (8)$$

In Fig. 5, the crosstalk identification from the FSM's  $\phi$ -axis to the MP's translational DoF  $z$  is exemplarily shown. By measuring  $\frac{z}{u_\phi S_z} = K_{\phi \rightarrow z} G_z$  (dashed-dotted red) and correcting the result by the known MP dynamics  $G_z$  (black), the gain  $K_{\phi \rightarrow z}$  (solid red) between the FSM's controller output  $u_\phi$  and the MP position  $z$  is obtained. As can be seen,  $K_{\phi \rightarrow z}$  shows the expected constant behavior for scan frequencies up to 200 Hz.

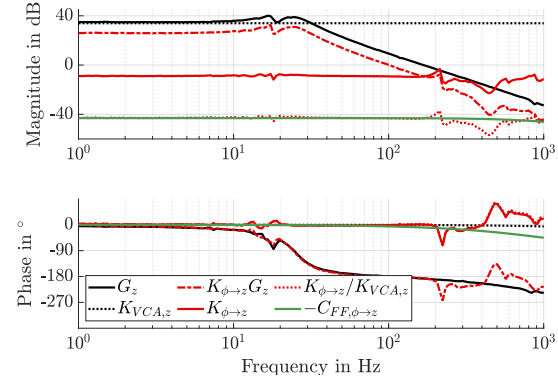


Fig. 5: Crosstalk identification from the FSM's  $\phi$ -axis to the translational MP position  $z$  and FF controller design to compensate the FSM motion-induced cross coupling.

##### B. Feedforward control design

Based on the previously identified crosstalk dynamics, a FF controller  $\mathbf{C}_{\text{FF}}$  (see Fig. 4) is designed in order to compensate the FSM-induced reaction forces acting on the MP. The entire MP position can be written as

$$\zeta = \underbrace{(\mathbf{u}_{\text{MP}} + \mathbf{u}_{\text{FF}}) \mathbf{K}_{\text{VCA}} + \mathbf{F}_{\text{FSM} \rightarrow \text{MP}}}_{\perp \mathbf{u}_{\text{MP}}} \mathbf{G}_{\text{MP}}, \quad (9)$$

with  $\mathbf{u}_{\text{FF}} = \mathbf{C}_{\text{FF}} \mathbf{u}_{\text{FSM}}$  the FF controller output. Using Eq. (6), the FF controller

$$\mathbf{C}_{\text{FF}} = -\frac{\mathbf{K}_{\text{F,FSM}} \mathbf{K}_{\text{HRA}}}{\mathbf{K}_{\text{VCA}}} \quad (10)$$

is obtained in order to achieve the desired dynamic MP behavior  $\zeta = \mathbf{u}_{\text{MP}} \mathbf{G}_{\text{MP}}$ .

Applying the FF controller design from Eq. (10) to the identified FSM motion-induced cross coupling ( $\phi \rightarrow z$ ) in Fig. 5 yields the relation  $K_{\phi \rightarrow z} / K_{\text{VCA},z}$  in dotted red, with  $K_{\text{VCA},z}$  (dashed-dotted black) being the gain of the VCA system in DoF  $z$ . With consideration of the maximum FSM Lissajous scanning frequencies ( $f_\phi = 59 \text{ Hz}$ ,  $f_\phi = 47 \text{ Hz}$ ),  $K_{\phi \rightarrow z} / K_{\text{VCA},z}$  is fitted by a first order low-pass with a gain of  $-43 \text{ dB}$  and a cut-off frequency of  $1 \text{ kHz}$ , yielding the frequency response of the desired FF controller  $C_{\text{FF},\phi \rightarrow z}$  (solid green). Following the same controller synthesis for the FSM's  $\theta$ -axis-induced cross coupling  $K_{\theta \rightarrow z}$ , the final FF controller

$$\mathbf{C}_{\text{FF},z} = \begin{bmatrix} C_{\text{FF},\theta \rightarrow z} & 0 \\ 0 & C_{\text{FF},\phi \rightarrow z} \end{bmatrix} \quad (11)$$

is integrated into the overall measurement module's control architecture, aiming to improve the sample-tracking performance in the MP's DoF  $z$  during SCCS operation (see Tab. I).

## V. EXPERIMENTAL SYSTEM PERFORMANCE EVALUATION

To investigate the performance improvement by the integrated FF compensation of the FSM-induced reaction forces, the robotic 3D measurement system is aligned to the sample holder [17]. A calibration standard (Nanuler Calibration Standard, Applied NanoStructures Inc., Mountain view, CA, USA) with a structural height of  $5.81 \mu\text{m}$  is used as sample surface under test.

### A. Increase of sample-tracking performance

With the MP being actively tracking the sample surface, the sample-tracking error is evaluated during the operation of the SCCS at maximum frame rate, i.e. applying Lissajous scanning frequencies  $f_\phi = 59 \text{ Hz}$  and  $f_\theta = 47 \text{ Hz}$  to the FSM. The tracking error obtained in the time domain for the conventional, purely FB-controlled operation of the measurement module is shown in Fig. 6 (black). As can be seen, the individual disturbance components generated by actuation of the FSM axes and the resulting reaction forces superimpose, yielding a beat frequency of  $\Delta f = f_\phi - f_\theta = 12 \text{ Hz}$  and a tracking error of  $290 \text{ nm rms}$ . Repeating the same measurement for the additionally enabled FF compensation of the FSM-induced reaction forces, the tracking error in red is obtained. With a residual tracking error of  $42 \text{ nm rms}$ , the sample-tracking performance is significantly increased by a factor of 7. Compared to the MP's static positioning noise of  $30 \text{ nm rms}$  (see Tab. I), the tracking error is reduced to the same order of magnitude.

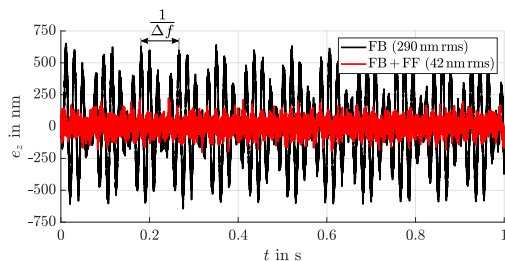


Fig. 6: Sample-tracking error in DoF  $z$  for the SCCS operating at the maximum frame rate of 1 fps. For the purely FB-controlled operation (black), the disturbances induced by the scanning FSM axes superimpose, yielding beats with a frequency of  $\Delta f = 12 \text{ Hz}$ . The additional FF control reduces the RMS tracking error from  $290 \text{ nm}$  to  $42 \text{ nm}$  (red).

### B. Improvement of 3D measurement uncertainty

Finally, the 3D measurement improvement by the additional FF approach for compensation of the FSM-induced reaction forces is evaluated. With consideration of the experiments performed in Section V-A, the according 3D measurement results of a structural step with a height of  $5.81 \mu\text{m}$  are shown in Fig. 7. For disabled FF control (Fig. 7a), the

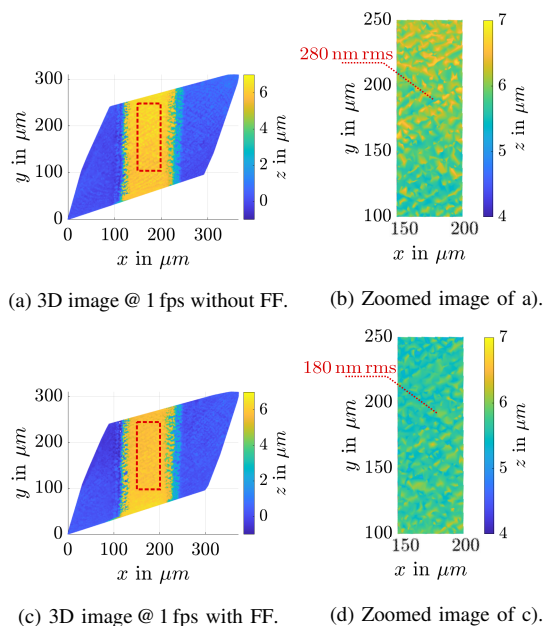


Fig. 7: 3D imaging performance evaluation on a structural step. a) and c) show the 3D measurement results at a frame rate of 1 fps for disabled and enabled FF control. By analyzing the dashed red area in b) and d), the RMS measurement uncertainty in the structural height is reduced from  $280 \text{ nm}$  to  $180 \text{ nm}$ .

measurement uncertainty in the structural height ( $z$ ) within the flat scan area (dashed red) is evaluated to  $280 \text{ nm rms}$  (Fig. 7b). By analyzing the according 3D measurement result for enabled FF control, the structural height uncertainty in the same scan area is reduced to  $180 \text{ nm rms}$ , equalling an increase in the 3D measurement uncertainty by  $1 - \frac{180 \text{ nm}}{280 \text{ nm}} = 36\%$

In summary, the proposed FF control scheme for the robotic 3D measurement system significantly reduces the disturbances caused by the FSM-induced reaction forces acting on the MP, reducing the sample-tracking error by a factor of 7 down to  $42 \text{ nm rms}$  and improving the 3D measurement uncertainty by 36%.

## VI. CONCLUSION

This paper proposes a FF control approach for an active-sample tracking 3D measurement module, which acts as a robotic end-effector and is targeted for precise robotic measurement applications directly in the vibration-prone environment of an industrial production line. By means of a FB control-induced stiff link, a constant position of the electromagnetically levitated and actuated MP with respect to the sample surface under test is maintained. In this way, lab-like conditions for the embedded SCCS are established, which is capable of performing precision 3D measurements with frame rates up to 1 fps. The SCCS includes a 2D FSM

to precisely scan the measuring light spot of a 1D CCS across the sample surface. Based on the identified disturbance dynamics of the FSM-induced reaction forces acting on the sample-tracking MP, a tailored FF control is synthesized and implemented. Experimental results successfully proof the targeted compensation of the disturbances caused by the operating SCCS. In the time domain, the sample-tracking error in the MP's translational DoF  $z$  is reduced by a factor of 7 down to 42 nm rms, which is close to the MP's static positioning noise. The reduced sample-tracking error further improves the 3D measurement performance of the SCCS operating at 1 fps by reducing the structural height uncertainty by 36% down to 180 nm rms.

#### ACKNOWLEDGMENT

This project is partially funded by the Hochschuljubilaeumsfonds of the city of Vienna, Austria under the project number H-260744/2020. The financial support by the Austrian Federal Ministry for Digital and Economic Affairs, and the National Foundation for Research, Technology and Development, as well as MICRO-EPSILON MESSTECHNIK GmbH & Co. KG and ATENSOR Engineering and Technology Systems GmbH is gratefully acknowledged.

#### REFERENCES

- [1] D. Imkamp, R. Schmitt, and J. Berthold, "Blick in die Zukunft der Fertigungsmesstechnik - Die VDI/VDE-GMA Roadmap Fertigungsmesstechnik 2020." *Technisches Messen*, vol. 10, no. 79, 2012.
- [2] T. Uhrmann, T. Matthias, M. Wimplinger, J. Burggraf, D. Burgstaller, H. Wiesbauer, and P. Lindner, "Recent progress in thin wafer processing," in *2013 IEEE International 3D Systems Integration Conference (3DIC)*, 2013, pp. 1–8.
- [3] R. Schmitt and F. Moenning, "Ensure success with inline-metrology," in *XVIII IMEKO World Congress - Metrology for a Sustainable Development*, 2006.
- [4] H. Schwenke, U. Neuschaefer-Rube, T. Pfeifer, and H. Kunzmann, "Optical methods for dimensional metrology in production engineering," *CIRP Annals*, vol. 51, no. 2, pp. 685–699, 2002.
- [5] W. Gao, H. Haitjema, F. Fang, R. Leach, C. Cheung, E. Savio, and J. Linares, "On-machine and in-process surface metrology for precision manufacturing," *CIRP Annals*, vol. 68, no. 2, pp. 843 – 866, 2019.
- [6] M. Grasso and B. Colosimo, "Process defects and in situ monitoring methods in metal powder bed fusion: a review," *Measurement Science and Technology*, vol. 28, p. 044005, 2017.
- [7] E. Savio, L. D. Chiffre, and R. Schmitt, "Metrology of freeform shaped parts," *CIRP Annals*, vol. 56, no. 2, pp. 810 – 835, 2007.
- [8] A. Yogeswaran and P. Payeur, "3d surface analysis for automated detection of deformations on automotive body panels," in *New Advances in Vehicular Technology and Automotive Engineering*. IntechOpen, 2012.
- [9] T.-F. Yao, A. Duenner, and M. Cullinan, "In-line dimensional metrology in nanomanufacturing systems enabled by a passive semiconductor wafer alignment mechanism," *Journal of Micro- and Nano-Manufacturing*, vol. 5, no. 1, 2016.
- [10] J. Rejc, J. Cinkelj, and M. Munih, "Dimensional measurements of a gray-iron object using a robot and a laser displacement sensor," *Robotics and Computer-Integrated Manufacturing*, vol. 25, no. 2, pp. 155–167, 2009.
- [11] E. Csencsics, M. Thier, S. Ito, and G. Schitter, "Supplemental peak filters for advanced disturbance rejection on a high precision endeffector for robot-based inline metrology," *IEEE/ASME Transactions on Mechatronics (Early Access)*, pp. 1–1, 2021.
- [12] U. Schneider, M. Drust, M. Ansaloni, C. Lehmann, M. Pellicciari, F. Leali, J. Gunnink, and A. Verl, "Improving robotic machining accuracy through experimental error investigation and modular compensation," *The International Journal of Advanced Manufacturing Technology*, vol. 85, pp. 1–13, 2014.
- [13] S. Yin, Y. Ren, Y. Guo, J. Zhu, S. Yang, and S. Ye, "Development and calibration of an integrated 3d scanning system for high-accuracy large-scale metrology," *Measurement*, vol. 54, pp. 65–76, 2014.
- [14] G. B. de Sousa, A. Olabi, J. Palos, and O. Gibaru, "3d metrology using a collaborative robot with a laser triangulation sensor," *Procedia Manufacturing*, vol. 11, pp. 132–140, 2017.
- [15] R. Saathof, M. Thier, R. Hainisch, and G. Schitter, "Integrated system and control design of a one dof nano-metrology platform," *Mechatronics*, vol. 47, pp. 88 – 96, 2017.
- [16] D. Wertjan, E. Csencsics, T. Kern, and G. Schitter, "Bringing the lab to the fab: Robot-based inline measurement system for precise 3-d surface inspection in vibrational environments," *IEEE Transactions on Industrial Electronics*, vol. 69, no. 10, pp. 10 666–10 673, 2022.
- [17] D. Wertjan, T. Kern, A. Pechhacker, E. Csencsics, and G. Schitter, "Robotic precision 3d measurements in vibration-prone environments enabled by active six dof sample-tracking," in *2022 IEEE/ASME International Conference on Advanced Intelligent Mechatronics (AIM)*, 2022, pp. 1441–1446.
- [18] D. Wertjan, T. Kern, E. Csencsics, G. Stadler, and G. Schitter, "Compact scanning confocal chromatic sensor enabling precision 3-d measurements," *Appl. Opt.*, vol. 60, no. 25, pp. 7511–7517, 2021.
- [19] Y. Jiang, Y. Zhu, K. Yang, C. Hu, and D. Yu, "A data-driven iterative decoupling feedforward control strategy with application to an ultra-precision motion stage," *IEEE Transactions on Industrial Electronics*, vol. 62, no. 1, pp. 620–627, 2015.
- [20] A. Sinn, S. Schachner, T. Riel, C. Schwaer, and G. Schitter, "Feed-forward vibration compensation for small telescopes," in *Advances in Optical and Mechanical Technologies for Telescopes and Instrumentation V*, vol. 12188, International Society for Optics and Photonics. SPIE, 2022, p. 121883H.
- [21] M. Beijen, M. Heertjes, J. Van Dijk, and W. Hakvoort, "Self-tuning mimo disturbance feedforward control for active hard-mounted vibration isolators," *Control Engineering Practice*, vol. 72, pp. 90–103, 2018.
- [22] E. Csencsics and G. Schitter, "Design of a phase-locked-loop-based control scheme for lissajous-trajectory scanning of fast steering mirrors," in *2017 American Control Conference (ACC)*, 2017, pp. 1568–1573.
- [23] M. Heertjes and A. van Engelen, "Minimizing cross-talk in high-precision motion systems using data-based dynamic decoupling," *Control Engineering Practice*, vol. 19, no. 12, pp. 1423–1432, 2011.
- [24] D. Wertjan, E. Csencsics, J. Schlarp, and G. Schitter, "Design and control of a maglev platform for positioning in arbitrary orientations," in *2020 IEEE/ASME International Conference on Advanced Intelligent Mechatronics (AIM)*, 2020, pp. 1935–1942.
- [25] E. Csencsics, J. Schlarp, T. Schopf, and G. Schitter, "Compact high performance hybrid reluctance actuated fast steering mirror system," *Mechatronics*, vol. 62, p. 102251, 2019.